A heavyweight early whale pushes the boundaries of vertebrate morphology

Giovanni Bianucci[1], Olivier Lambert[2], Mario Urbina[3], Marco Merella[1], Alberto Collareta[1], Rebecca Bennion[2,4], Rodolfo Salas-Gismondi[3,5], Aldo Benites-Palomino[3,6], Klaas Post[7], Christian de Muizon[8], Giulia Bosio[9], Claudio Di Celma[10], Elisa Malinverno[9], Pietro Paolo Pierantoni[10], Igor Maria Villa[11], Eli Amson[12,]*

1. Dipartimento di Scienze della Terra, Università di Pisa, 56126 Pisa, Italy
2. D.O. Terre et Histoire de la Vie, Institut royal des Sciences naturelles de Belgique, 1000 Brussels, Belgium
3. Departamento de Paleontología de Vertebrados, Museo de Historia Natural-Universidad Nacional Mayor de San Marcos, Lima 11, Perú
4. Evolution & Diversity Dynamics Lab, UR Geology, Université de Liège, 4000 Liège, Belgium
5. Facultad de Ciencias y Filosofía/Centro de Investigación para el Desarrollo Integral y Sostenible, Laboratorios de Investigación y Desarrollo, Universitad Peruana Cayetano Heredia Lima, Perú
6. Department of Paleontology, University of Zurich, 8006 Zurich, Switzerland
7. Natuurhistorisch Museum Rotterdam, Rotterdam 3001 KL, The Netherlands
8. CR2P (CNRS, MNHN, Sorbonne Université), Département Origines et Évolution, Muséum national d’Histoire naturelle, F-75231 Paris cedex 05, France
9. Dipartimento di Scienze dell’Ambiente e della Terra, Università degli Studi di Milano-Bicocca, 20126, Milano, Italy
10. School of Science and Technology, University of Camerino, 62032 Camerino, Italy
11. Institut für Geologie, Universität Bern, 3012 Bern, Switzerland
12. Staatliches Museum für Naturkunde Stuttgart DE-70191 Stuttgart, Germany

*corresponding author

Summary paragraph

The fossil record of cetaceans documents how terrestrial animals acquired extreme adaptations and transitioned to a fully aquatic lifestyle[1,2]. In whales, this is associated with a dramatic increase in maximum body size. While an elongate body was acquired early in cetacean evolution[3], the maximum body mass of baleen whales reflects a recent diversification that culminated with the blue whale[4]. More generally, hitherto known gigantism among aquatic tetrapods evolved within pelagic, active swimmers. Here we describe *Perucetus colossus*, a new basilosaurid whale from the middle Eocene of Peru. It displays the strongest degree of bone mass increase known to date, an adaptation associated with shallow diving[5]. This species' estimated skeletal mass exceeds that of any known mammal or aquatic vertebrate. We show that the bone structure specialisations of aquatic mammals are reflected in the scaling of skeletal fraction (skeletal mass versus whole body mass) across the entire disparity of amniotes. We use skeletal fraction to estimate the body mass of *Perucetus colossus*, who proves to be a contender to the title of heaviest animal on record. Cetaceans' peak body mass had already been reached ca. 30 million years before previously assumed, in a coastal context where primary productivity was particularly high.

Main text

The fossil record of cetaceans provides one of the most striking documentations of an evolutionary transition of lifestyle[1,2]. This transition brought a fully terrestrial group of mammals back to water, over 300 million years after tetrapods first gained ground[6]. Early to middle Eocene artiodactyls with a chevrotain-like morphology (e.g., *Indohyus*) are understood to be the closest known relatives of cetaceans[7]. Becoming increasingly specialised to aquatic life during this global greenhouse stage, cetaceans quickly evolved larger body sizes, with a first significant trend of body elongation seen in late Eocene basilosaurines[8]. The true gigantism and associated body mass seen in baleen whales is nevertheless a recent acquisition, probably associated with the cooling trend and seasonality installed in the late Cenozoic[4]. Furthermore, the largest cetacean is the extant blue whale (*Balaenoptera musculus*), which is also the heaviest animal hitherto known. More generally, the largest taxa among aquatic tetrapods (which include marine reptiles such as ichthyosaurs[9]) known so far are all pelagic, active swimmers.

As animals acquire more aquatic habits, buoyancy becomes a critical aspect of their biology. Bone is dense relative to most other tissues and present in large quantities in the tetrapod body, which likely explains why bone mass specialisations are documented in a myriad of tetrapod lineages that independently evolved aquatic habits[10]. Shallow-diving, slow-swimming species' adaptations often comprise bone mass increase (BMI). This is produced by the infilling of skeletal elements' inner cavities with compact bone (i.e., osteosclerosis) and, in the more extreme cases, by additional deposition of bone on their external surface[5] (i.e., pachyostosis *sensu stricto*). BMI is documented in cetaceans' amphibious close relatives[11], as well as early members of the clade, the basilosaurids in particular. Extant cetaceans have conversely acquired an entirely different bone microanatomy, with an osteoporotic-like structure typical of pelagic, secondarily aquatic tetrapods with more active swimming. Basilosaurids are therefore unique in the sense that they acquired large sizes (up to ca. 20 m in body length[3]) and BMI. The degree of their BMI nevertheless did not match, up until now, that of some sirenians for instance, where the whole rib cage is both strongly osteosclerotic and pachyostotic[5].

Here we describe a new basilosaurid whale that drastically pushes the upper limit of skeletal mass in mammals, as well as in aquatic vertebrates in general. This early whale combines a gigantic size and the strongest degree of BMI known to date. It also potentially represents the heaviest animal ever described.

Systematic palaeontology

Cetacea Brisson, 1762

Archaeoceti Flower, 1883

Pelagiceti Uhen, 2008

Basilosauridae Cope, 1868

Perucetus colossus gen. et sp. nov.

Etymology. From Peru, the country of origin of the holotype and Latin *cetus* (whale). Species epithet from the Ancient Greek *kolossós* (large statue and by extension any creature of gigantic size and mass).

Holotype. MUSM 3248 (Museo de Historia Natural, Universidad Nacional Mayor de San Marcos, Lima, Peru), a partial skeleton including 13 vertebrae (two tentatively referred to the last thoracics named here Th-a and Th-b and the others to the anterior lumbars named here L-a - L-k), four ribs, and right innominate lacking the distal portion of the ilium (Fig. 1, Extended Data Figs. 2-5). The animal was likely approaching skeletal maturity (see Supplementary Discussion, Bone histology).

Locality and horizon. From the upper part of the Yumaque member of the Paracas Formation exposed in the Ica valley a few kilometres south of the Zamaca locality, Ica Province, southern Peru[12] (Extended Data Fig. 1). Its geological age is well constrained between 39.8-37.84 million years ago

(Bartonian, middle Eocene) through biostratigraphy and ^{39}Ar-^{40}Ar dating on tephra layer. Coordinates for the type locality are available on request through the corresponding author. See Methods, Extended Data Fig. 1 and Supplementary Methods for more geological and palaeoenvironmental information and detailed justification of the age.

Diagnosis. *Perucetus colossus* differs from all other cetaceans by having an extremely pachyosteosclerotic postcranium. Pachyosteosclerosis is also present in a few other cetaceans[13,14], including the basilosaurid Pachycetinae[15], but to a significantly lesser degree than observed in this new taxon. *P. colossus* belongs to Pelagiceti by having a high number of lumbars (at least 11), an extremely reduced innominate, and centra of the last two thoracics and preserved lumbars with a roughly circular cross-section (CH/CW > 0.80), not dorsoventrally compressed nor heart-shaped (as observed instead in the more stemward archaeocetes). Within Pelagiceti, *P. colossus* shares with *Basilosaurus*, *Chrysocetus*, *Cynthiacetus peruvianus*, *Mystacodon* and *Pachycetus wardii* a plesiomorphic, well-defined acetabulum on the innominate, but differs from *Basilosaurus*, *Chrysocetus* and *Mystacodon* and probably *Pachycetus* by the more robust proximal portion of the ilium, and from *Basilosaurus* by the larger obturator foramen and the overall shape of the innominate, which is triangular in profile view. *P. colossus* differs from all cetaceans but Basilosaurinae and Pachycetinae by the great elongation of the centra of the lumbars (CL/CW = 1.25-1.56), approaching the values seen in *Pachycetus* and *Antaecetus* (CL/CW = 1.30-1.68); more extreme values are observed in *Basilosaurus* (CL/CW = 169-1.98) (Extended Data Fig. 6). *P. colossus* shares with *Basilosaurus* the giant size (CW > 20 cm) and club-like shape of the distal end of at least some of the ribs. Estimated skeletal length: ca. 17-20 m (see Supplementary Methods and Fig. S7).

The assignation of the vertebrae to the last two thoracic and the first 11 lumbar positions is based on the ventral position of the transverse processes, the large neural canals (although reduced due to the pachyostosis of the neural arches), and the lack of foveae for the capitula of the ribs. The transverse processes are significantly bent ventrolaterally, similarly to the lumbars of other basilosaurids[16–18].

Moreover, all the distal portions of the transverse processes exhibit a peculiar wide, oval, flattened area on their ventral surface (Fig. 1j; Extended Data Figs. 2-5). The two thoracic vertebrae also bear a concavity at the anterolateral tip of their transverse processes, where the last ribs likely articulated. These two vertebrae are also distinguished by their neural spine, which is more slender and with a dorsal edge sloping posteriorly.

For roughly half of the recovered vertebrae, either one or both of the centrum epiphyses are missing, suggesting partial epiphyseal fusion. This should not be seen as a sign of immaturity for the specimen, as some large, extant cetaceans maintain their thoracic and lumbar centrum epiphyses unfused late into adulthood[19].

The best preserved rib displays a simple proximal end without distinct tuberculum and capitulum and a weak overall curvature in anterior or posterior view (Fig. 1e,f; Extended Data Fig. 6c; Supplementary Data 1). This morphology (also observed in the other three preserved ribs) is consistent with a rib of the posterior region (R17-20), which would entail that the whole rib cage was likely pachyostotic in *P. colossus*, contrary to other basilosaurids[16,17,20].

The heaviest mammalian skeleton

The extreme skeletal morphology of the new species is not pathological. First, bone mass increase (BMI) is part of the healthy phenotype expressed in many aquatic tetrapods[10]. It is common in basilosaurids, and pachyosteosclerosis is even considered as a diagnostic feature of one of its subfamilies, the pachycetines[15]. Secondly, in conditions involving additional bone deposition such as acromegaly or osteopetrosis, both gross morphology and bone inner structure alterations are highly variable, both within a single bone and across the skeleton[21,22]. In contrast, in aquatic tetrapods with BMI (including *P. colossus*), skeletal elements are uniformly affected by these alterations. Finally, in *P. colossus*, the pachyostosis affects all the bones that have been recovered (vertebrae, ribs and innominate). It is most conspicuous in the strongly bloated apophyses of the vertebrae, which hence strikingly differ from those of the vast majority of mammals (Figs. 1-2, Extended Data Figs. 2-5). All extant cetaceans, including the largest balaenopterids and balaenids, show the usual, relatively thin vertebral apophyses[23]. Pachyostosis increases significantly the volume of the new species' vertebrae, which represents almost twice that of the largest vertebra of a 25-m long blue whale (Fig. 2; Supplementary Table 1). The recovered ribs are also entirely pachyostotic (Fig. 1e-f, Extended Data Fig. 5m). We estimate *P. colossus*' total skeletal volume (using that of the preserved elements and virtually complete skeletons of other basilosaurids as well as a conservative vertebral count) to be 2.9-4.1 m^3. Scaling up the vertebrae of *Cynthiacetus peruvianus*, a smaller, non-pachyostotic close relative, it can be estimated that the pachyostosis of *P. colossus* results in an excess of over 350 % in overall volume (Supplementary Methods).

The bone microanatomy of *P. colossus* is also consistent with an extreme case of BMI: all observed break surfaces and histological samples indicate strong osteosclerosis (Fig. 3; Extended Data Fig. 7; Supplementary Discussion and Table 2). The rib is entirely made of compact bone, lacking a medullary region altogether. Growth marks (annuli) indicate strong cortical drift, with the original growth centre positioned in the current medial-most edge of the bone. A similar but weaker bone drift is seen in *Basilosaurus*[13,24]. Histological sections of both the vertebrae and rib show a very consistent reticular woven-parallel complex devoid of remodelling, making up most of the skeletal elements. The network of primary osteons is extremely dense and convoluted (Fig. 3). The vascular canals themselves are very narrow (most primary osteons are mature with a small lumen), increasing further the compactness of the bone tissue. The same type of bone tissue is described for the rib cortex of *Basilosaurus*, but in the latter various degrees of primary osteon completion are observed, resulting in a less compact cortex[24]. As pachyostosis, osteosclerosis is therefore generalised, too. The fact that all recovered elements (including the strongly reduced innominate) are affected by BMI suggests that the responsible process acted systemically, as already argued for some other marine mammals with BMI[25].

We estimated the total skeletal mass of *P. colossus* combining the skeletal volume to the skeletal elements' density (based on palaeohistological samples; Supplementary Methods). With estimates ranging from 5.3 to 7.6 tonnes (Supplementary Table 22), the skeleton weighed 2.0-2.9 times as much as that of a 25-m long blue whale (Supplementary Table 6).

Skeletal mass across amniotes

The repeated acquisition of bone mass increase in aquatic amniotes underlines the importance for these animals of body trim and overall density[26], which are defined by the distribution and mass of skeletal and soft tissues. To assess how skeletal fraction (ratio of skeletal and total body mass, SF) relates to lifestyle and body size, we examined the scaling of dry skeletal mass in a sample of mammals with known body masses (Fig. 4; Supplementary Tables 3-4; Supplementary Data 2). Compared to terrestrial mammals, cetaceans have a relatively lighter skeleton, with SF values ranging from 2.2 to 5.1%. In terrestrial mammals, skeletal mass scales with positive allometry, and SF ranges from 4 to 10%. The skeletal mass in amniotes actually spans nine orders of magnitude (our estimates range from 26 milligrams for the dwarf chameleon *Brookesia nana* to 9.9 tonnes for the sauropod *Argentinosaurus huinculensis*). The skeletal mass of extant sirenians essentially scales as that of terrestrial mammals. These differences of scaling emphasise the two types of aquatic specialisations described in extant cetaceans and sirenians, the osteoporotic-like condition and BMI, respectively[5].

Estimating body mass in basilosaurids is challenging[27]. For *P. colossus*, methods based on simple skeletal measurements would also likely be biased by the fact that its skeletal morphology starkly departs from that of other marine mammals. Furthermore, the excess of skeletal mass might have been compensated for by large amounts of blubber (less dense than most other soft tissues in amniotes), which in turn would strongly affect the overall density of soft tissues. But the scaling relationships described above, which can be used to estimate body mass based on skeletal mass, are indicative of the viable SF values found in fully aquatic mammals (as for all other aquatic amniotes the necessity of frequent surfacing to breathe prevents any strong deviation from neutral buoyancy). Given the two patterns observed for the SF of fully aquatic mammals, we have used the extreme values measured in extant sirenians and cetaceans: assuming the mean SF of adult manatees (extant marine mammals with the strongest BMI) and the minimum skeletal volume estimation yields a body mass of 85 tonnes for *P. colossus*. Using extant cetaceans' lowest SF and the maximum skeletal volume yields an estimation of 340 tonnes (Supplementary Table 22). With the mean of the skeletal mass estimates and the mean cetacean SF (3.6%), an estimated body mass of 180 tonnes is obtained. These estimates fall in or exceed the body mass distribution of the blue whale[28], which hence challenges the latter species' title of heaviest animal that ever existed.

***Perucetus*' lifestyle and the evolution of cetacean gigantism**

The combination of extreme pachyostosis and osteosclerosis displayed by *P. colossus* is only approached by tetrapod species that are adapted to a fully aquatic lifestyle, as it would make movement on land overly problematic due to gravity[29,30]. Coupled with the greatly reduced size of the innominate, this observation confirms that *P. colossus* did not return to land, not even to give birth. The extreme pachyosteosclerosis of *P. colossus* is only consistent with a shallow-water lifestyle, wherein it would have contributed to the buoyancy control, as in extant sirenians[26,31].

Such a large and heavy animal may also have been able to counteract waves in high-energy waters[30,32], as also hypothesised for the giant, recently extinct Steller's sea cow, *Hydrodamalis gigas*[29]. A coastal habitat has already been proposed for basilosaurids based on stable isotopes and skeletal anatomy[33,34].

The elongate centra of the vertebrae of *P. colossus* is a character that, in other basilosaurids, has been related to swimming by means of axial undulation[15,35,36]. Such a swimming style is practiced by the extant manatees (*Trichechus* spp.), contrasting with the caudal oscillation seen in the dugong (*Dugong dugon*), who is less affected by BMI and who occupies more open water habitats[37]. Extant cetaceans' carangiform with lunate-tail swimming also involves such oscillations[38]. Extreme pachyostosis would have restricted the movements between adjacent vertebrae, thus further constraining the swimming style to low amplitude undulations[10]. Indeed, the extensive anteroposterior widening of the transverse processes and neural spine that characterises all the preserved vertebrae of *P. colossus* should have severely limited the flexural capabilities of the vertebral column. To test this assumption, we followed the methodology of Molnar et al.[39], evidencing that the maximum degrees of dorsal and -especially- lateral flexion were very low in *P. colossus* compared to *Cynthiacetus peruvianus*; in turn, the capability of ventral flexion was instead higher (Extended Data Fig. 8). This suggests that *P. colossus*, like *Antaecetus* and *Pachycetus*[15], swam with a slow dorsoventral undulation of the posterior part of the body, without involving any degree of mediolateral undulation as proposed instead for *Basilosaurus*[35,36,40]. A strong ventral flexion may have helped to push the heavy body of *P. colossus* upwards from the seafloor to breathe at the surface. Gigantism combined with the inferred undulatory swimming style of *P. colossus* and *Basilosaurus* could represent an evolutionary adaptation analogous to that observed in Triassic ichthyosaurs. Indeed, in these marine reptiles a giant size has been proposed to compensate for the relatively high energetic cost of undulatory locomotion[41]. It is also noteworthy that a generalised pachyostosis in the axial postcranium is otherwise found in much smaller (about 1 metre or less) aquatic reptiles[42]. These taxa also purportedly used undulatory locomotion, as suggested by their serpentiform body plan. There may thus be similar selective pressures resulting in the convergent reduction of the limbs and acquisition of an elongate body with strong bone mass increase of the axial postcranium in aquatic tetrapods. Gigantism could also have been selected to allow for longer dives near the sea bottom in shallow waters. Indeed, dive duration in air-breathing vertebrates displays a strong allometric relationship with body mass[43].

Since the skull and teeth of *P. colossus* are unknown, any hypothesis about its diet and feeding strategy of this idiosyncratic early whale would be speculative. However, having hypothesised slow swimming speeds as well as benthic habits in shallow and agitated waters (Extended Data Fig. 10), and considering the huge quantity of food that would be needed to sustain such a giant animal, several observations may be made regarding the feeding style of *P. colossus*. Similar to sirenians, *P. colossus* may have fed on seagrass and/or seaweed, but that would make it the sole herbivorous cetacean, a rather unlikely scenario. Alternatively, *P. colossus* may have fed on benthic, sedentary or sessile fauna (e.g., crustaceans, demersal fishes, molluscs, etc.). Suction- and/or filter-feeding strategies to forage benthic fauna could also be speculatively evocated, in analogy with the trophic habits of the extant grey whale (*Eschrichtius robustus*). Finally, a further conjectural hypothesis is that *P. colossus* fed on low-cost, high-energy food sources by means of scavenging upon sunken vertebrate carcasses, similar to many extant large-bodied demersal sharks. Unfortunately, the sedimentological data and the scarce associated fauna do not provide useful information to better define the palaeoecology of *P. colossus*, its carcass having been probably transported to relatively deeper waters, though not far away from the coast (Supplementary Methods).

In summary, the morphology and microanatomy of *Perucetus colossus* extend the gamut of known skeletal phenotypes, which in turn alters our understanding of mammalian maximum body mass evolution. The order of magnitude of 10^5 kg has not only been reached recently, in Neoceti (crown group cetaceans), but likely during the Bartonian, an age of cetacean evolution characterised by mild to extreme bone mass increase. The second half of the Eocene was also a time when a peak in maximum body mass was already observed in other mammalian clades[44,45]. While uncertainties remain regarding the precise lifestyle and diet of *P. colossus*, it was a slow-swimming, most likely coastal, benthic consumer which further suggests that the pelagic adaptations of Neoceti (and other large marine tetrapods) are not a prerequisite to reach such large body masses. The ecological specialisation associated with the extreme skeletal morphology of *P. colossus* indicates some further degree of niche expansion[46] for Eocene cetaceans, in relation to the reduced gravitational constraints on size due to life in the water[47] and the high seafloor productivity at that time[48]. This new record supports the hypothesis that basilosaurids have hyper-specialised to coastal habitats during the end of the Eocene, and that the subsequent major drop in the productivity of these environments[48] may have preferentially impacted these whales, giving way for their relatives (the ancestors of nowadays' whales and dolphins) who invaded more offshore habitats[33].

References

1. Fordyce, R. E. Cetacean Evolution. in *Encyclopedia of Marine Mammals (Third Edition)* (eds. Würsig, B., Thewissen, J. G. M. & Kovacs, K. M.) 180–185 (Academic Press, 2018). doi:10.1016/B978-0-12-804327-1.00088-1.

2. Gingerich, P. D. Evolution of whales from land to sea. *Proc. Am. Philos. Soc.* **156**, 309–323 (2012).

3. Voss, M., Antar, M. S. M., Zalmout, I. S. & Gingerich, P. D. Stomach contents of the archaeocete *Basilosaurus isis*: Apex predator in oceans of the late Eocene. *PLoS One* **14**, 1–24 (2019).

4. Slater, G. J., Goldbogen, J. A. & Pyenson, N. D. Independent evolution of baleen whale gigantism linked to Plio-Pleistocene ocean dynamics. *Proc. R. Soc. B Biol. Sci.* **284**, (2017).

5. Buffrénil, V. de, Canoville, A., D'Anastasio, R. & Domning, D. P. Evolution of sirenian pachyosteosclerosis, a model-case for the study of bone structure in aquatic tetrapods. *J. Mamm. Evol.* **17**, 101–120 (2010).

6. Clack, J. A. *Gaining Ground: the Origin and Evolution of Tetrapods*. (Indiana University Press, 2012).

7. Thewissen, J. G. M., Cooper, L. N., Clementz, M. T., Bajpai, S. & Tiwari, B. N. Whales originated from aquatic artiodactyls in the Eocene epoch of India. *Nature* **450**, 1190–4 (2007).

8. Burin, G., Park, T., James, T. D., Slater, G. J. & Cooper, N. The dynamic adaptive landscape of cetacean body size. *Curr. Biol.* 1–8 (2023) doi:10.1016/j.cub.2023.03.014.

9. Sander, P. M. *et al.* Early giant reveals faster evolution of large body size in ichthyosaurs than in cetaceans. *Science* **374**, (2021).

10. Houssaye, A., Martin Sander, P. & Klein, N. Adaptive patterns in aquatic amniote bone microanatomy—more complex than previously thought. *Integr. Comp. Biol.* **56**, 1349–1369 (2016).

11. Cooper, L. N. *et al.* Aquatic habits of cetacean ancestors: Integrating bone microanatomy and stable isotopes. *Integr. Comp. Biol.* **56**, 1370–1384 (2016).

12. Di Celma, C. *et al.* Towards deciphering the Cenozoic evolution of the East Pisco Basin (southern Peru). *J. Maps* **18**, 397–412 (2022).

13. Houssaye, A., Tafforeau, P., Muizon, C. de & Gingerich, P. D. Transition of Eocene whales from land to sea: evidence from bone microstructure. *PLoS One* **10**, e0118409 (2015).

14. Dewaele, L. *et al.* Hypersalinity drives convergent bone mass increases in Miocene marine mammals from the Paratethys. *Curr. Biol.* **32**, 248-255.e2 (2022).

15. Gingerich, P. D., Amane, A. & Zouhri, S. Skull and partial skeleton of a new pachycetine genus (Cetacea, Basilosauridae) from the Aridal Formation, Bartonian middle Eocene, of southwestern Morocco. *PLoS One* **17**, 1–43 (2022).

16. Kellogg, R. A review of the Archaeoceti. *Carnegie Inst. Washingt.* **482**, 1–366 (1936).

17. Uhen, M. D. Form, function, and anatomy of *Dorudon atrox* (Mammalia, Cetacea): an archaeocete from the middle to late Eocene of Egypt. *Univ. Michigan Pap. Paleontol.* **34**, 1–222 (2004).

18. Gingerich, P. D. *Stromerius nidensis*, new archaeocete (Mammalia, Cetacea) from the upper Eocene Qasr el-Sagha Formation, Fayum, Egypt. *Contrib. from Museum Paleontol. Univ.*

Michigan **31**, 363–378 (2007).

19. Moran, M. M. *et al.* Intervertebral and epiphyseal fusion in the postnatal ontogeny of cetaceans and terrestrial mammals. *J. Mamm. Evol.* **22**, 93–109 (2015).

20. Martínez-Cáceres, M., Lambert, O. & Muizon, C. de. The anatomy and phylogenetic affinities of *Cynthiacetus peruvianus*, a large *Dorudon*-like basilosaurid (Cetacea, Mammalia) from the late Eocene of Peru. *Geodiversitas* **39**, 7–163 (2017).

21. Anné, J., Tumarkin-Deratzian, A. R., Cuff, H. J., Orsini, P. & Grandstaff, B. Acromegaly in a Hog Badger (*Arctonyx collaris*). *Proc. Acad. Nat. Sci. Philadelphia* **167**, 85 (2019).

22. Gresky, J., Sokiranski, R., Witzmann, F. & Petiti, E. The oldest case of osteopetrosis in a human skeleton: exploring the history of rare diseases. *Lancet Diabetes Endocrinol.* **8**, 806–808 (2020).

23. Van Benenden, P.-J. & Gervais, P. *Ostéographie des cétacés*. (Arthus Bertrand, 1880).

24. Buffrénil, V. de, Ricqlès, A. de, Ray, C. E. & Domning, D. P. Bone histology of the ribs of the archaeocetes (Mammalia: Cetacea). *J. Vertebr. Paleontol.* **10**, 455–466 (1990).

25. Amson, E., Billet, G. & Muizon, C. de. Evolutionary adaptation to aquatic lifestyle in extinct sloths can lead to systemic alteration of bone structure. *Proc. R. Soc. B* **285**, 20180270 (2018).

26. Domning, D. P. & Buffrénil, V. de. Hydrostasis in the Sirenia: quantitative data and functional interpretations. *Mar. Mammal Sci.* **7**, 331–368 (1991).

27. Gingerich, P. D. Body weight and relative brain size (encephalization) in Eocene Archaeoceti (Cetacea). *J. Mamm. Evol.* **23**, 17–31 (2016).

28. Lockyer, C. Body weights of some species of large whales. *ICES J. Mar. Sci.* **36**, 259–273 (1976).

29. Taylor, M. A. Functional significance of bone ballastin in the evolution of buoyancy control strategies by aquatic tetrapods. *Hist. Biol.* **14**, 15–31 (2000).

30. Houssaye, A. ‘Pachyostosis’ in aquatic amniotes: a review. *Integr. Zool.* **4**, 325–40 (2009).

31. Ricqlès, A. de & Buffrénil, V. de. Bone histology, heterochronies and the return of tetrapods to life in water: were are we. in *Secondary adaptation of tetrapods to life in water* (eds. Mazin, J. & Buffrénil, V.) 289–310 (Verlag Dr Friedrich Pfeil, 2001).

32. Wall, W. P. The correlation between high limb-bone density and aquatic habits in recent mammals. *J. Paleontol.* **57**, 197–207 (1983).

33. Clementz, M. T., Goswami, A., Gingerich, P. D. & Koch, P. L. Isotopic records from early whales and sea cows: Contrasting patterns of ecological transition. *J. Vertebr. Paleontol.* **26**, 355–370 (2006).

34. Gingerich, P. D., Antar, M. S. M. & Zalmout, I. S. *Aegicetus gehennae*, a new late Eocene protocetid (Cetacea, Archaeoceti) from Wadi Al Hitan, Egypt, and the transition to tail-powered swimming in whales. *PLoS One* **14**, 1–55 (2019).

35. Gingerich, P. D., Smith, B. H. & Simons, E. L. Hind limbs of Eocene *Basilosaurus*: evidence of feet in whales. *Science* **249**, 154–157 (1990).

36. Buchholtz, E. A. Implications of Vertebral Morphology for Locomotor Evolution in Early Cetacea. in *The Emergence of Whales* 325–351 (1998). doi:10.1007/978-1-4899-0159-0_11.

37. Kojeszewski, T. & Fish, F. E. Swimming kinematics of the Florida manatee (*Trichechus manatus latirostris*): hydrodynamic analysis of an undulatory mammalian swimmer. *J. Exp. Biol.* **210**, 2411–8 (2007).

38. Fish, F. E. Comparative kinematics and hydrodynamics of odontocete cetaceans: Morphological and ecological correlates with swimming performance. *J. Exp. Biol.* **201**, 2867–2877 (1998).

39. Molnar, J. L., Pierce, S. E., Bhullar, B.-A. S., Turner, A. H. & Hutchinson, J. R. Morphological and functional changes in the vertebral column with increasing aquatic adaptation in

crocodylomorphs. *R. Soc. Open Sci.* **2**, 150439 (2015).

40. Gingerich, P. D. Land-to-sea transition in early whales: evolution of Eocene Archaeoceti (Cetacea) in relation to skeletal proportions and locomotion of living semiaquatic mammals. *Paleobiology* **29**, 429–454 (2003).

41. Gutarra, S. *et al.* Effects of body plan evolution on the hydrodynamic drag and energy requirements of swimming in ichthyosaurs. *Proc. R. Soc. B Biol. Sci.* **286**, (2019).

42. Wang, W., Shang, Q., Cheng, L., Wu, X. C. & Li, C. Ancestral body plan and adaptive radiation of sauropterygian marine reptiles. *iScience* **25**, 105635 (2022).

43. Verberk, W. C. E. P. *et al.* Universal metabolic constraints shape the evolutionary ecology of diving in animals. *Proc. R. Soc. B Biol. Sci.* **287**, 20200488 (2020).

44. Lovegrove, B. G. & Mowoe, M. O. The evolution of mammal body sizes: Responses to Cenozoic climate change in North American mammals. *J. Evol. Biol.* **26**, 1317–1329 (2013).

45. Baker, J., Meade, A., Pagel, M. & Venditti, C. Adaptive evolution toward larger size in mammals. *Proc. Natl. Acad. Sci. U. S. A.* **112**, 5093–5098 (2015).

46. Saarinen, J. *et al.* Patterns of maximum body size evolution in Cenozoic land mammals: eco-evolutionary processes and abiotic forcing. *Proc. R. Soc. B* **281**, 20132049 (2014).

47. Price, S. A. & Hopkins, S. S. B. The macroevolutionary relationship between diet and body mass across mammals. *Biol. J. Linn. Soc.* **115**, 173–184 (2015).

48. Vermeij, G. J. Shifting sources of productivity in the coastal marine tropics during the Cenozoic era. *Proc. R. Soc. B Biol. Sci.* **278**, 2362–2368 (2011).

Figure legends

Fig. 1 | **Partial skeleton of *Perucetus colossus* MUSM 3248, holotype. a**. Schematic body and skeletal reconstruction reporting the preserved bones (red). **b**,**c**. Right rib in anterior (**b**) and lateral (**c**) views. **d**-**f**. Right innominate in medial (**d**), dorsal (**e**), and lateral (**f**) views. **g**-**i**. Last preserved lumbar vertebra (L-k) in anterior (**g**), left lateral (**h**), and dorsal (**i**) views. **k**-**l**. Articulated sequence of the 13 collected vertebrae in dorsal (**j**), ventral (**k**), and right lateral (**l**) views. Scale bars, 50 cm (b,c,g-l) and 10 cm (d,e,f). All images were generated from 3D surface models.

Fig. 2 | **Pachyostosis in *Perucetus colossus* MUSM 3248, holotype. a, b**. Skeleton (**a**, preserved bones in dark grey), life reconstruction (**b**), and 3D models of a rib (**c**) and vertebra (L-k) of *P. colossus*. Skeletons (**e**, **h**), posterior rib (**f**, **i**) and last lumbar vertebra (**g**, **j**) of the Wexford blue whale (*Balaenoptera musculus*; **e**-**g**) and another basilosaurid, *Cynthiacetus peruvianus* (**h**-**j**). Scale bar for isolated bones, 50 cm; for skeletons and reconstruction, 2 m.

Fig. 3 | **Bone histology of *Perucetus colossus* MUSM 3248, holotype. a**. half rib cross-section (in three parts), featuring very sparse porosity and multiple growth marks (arrows). **b.** Detail of the above, showing a highly convoluted, woven-parallel complex, devoid of remodelling (left, natural light; right, cross-polarized light). **c**. Broken peduncle of a lumbar vertebra in ventral view (note fractures following growth lines), made of compact bone throughout. Small inset (vertebra parts in anterior view, not to scale) indicates position of the illustrated break surface. Scale bars, 1 cm (a), 0.5 mm (b), and 5 cm (c).

Fig. 4 | **Scaling of the skeletal mass across amniotes' body mass range.** Regressions based on extant, terrestrial mammals (grey line) and extant cetaceans (blue line). On the same graph are also plotted estimated values for extreme terrestrial amniotes, sirenians (either measured or estimated) as well as the result of our estimations for *Perucetus colossus*. Each data point corresponds to a distinct species (specific mean for the largest extant cetaceans, *Balaenoptera musculus* and *Physeter macrocephalus*), except for extant sirenians (represented by two species). Error bars indicate maximum and minimum estimates (some are too small to be visible). Scales are logarithmic. Human height, 1.8 m (scale for larger silhouettes); penny's diameter, 2 cm. See Supplementary Methods and Supplementary Data 2.

Extended Data Figures

Extended Data Fig. 1 | Location and stratigraphic position of *Perucetus colossus* MUSM 3248. a. Map showing the position of the Coastal Batholith and major trench-parallel structural highs along the coast of Peru (redrawn and modified after Travis et al.[79] and Thornburg & Kulm[80]). **b.** Stratigraphic column of the Cenozoic succession exposed in the East Pisco Basin (redrawn and modified after Malinverno et al.[81], Bianucci & Collareta[82], and Bosio et al.[83]). **c**. Measured stratigraphic section of the type locality of *P. colossus*, indicating the stratigraphic height of the holotype MUSM 3248, the dated tephra layer, and the identified bioevents.

Extended Data Fig. 2 | Three vertebrae of *Perucetus colossus* (MUSM 3248 holotype). a, g, m. Anterior view. **b, h, n.** Posterior view. **c, i, o.** Dorsal view. **d, j, p.** Ventral view. **e, k, q.** Right lateral view. **f, l, r.** Left lateral view. Tentative position along the vertebral column: **a-f** = Th-a, penultimate thoracic; **g-l** = Th-b, last thoracic; **m-r** = L-a, first lumbar. All images were generated from three-dimensional surface models. Scale bar = 50 cm.

Extended Data Fig. 3 | Three vertebrae of *Perucetus colossus* (MUSM 3248, holotype). a, g, m. Anterior view. **b, h, n.,** Posterior view. **c, i, o.** Dorsal view. **d, j, p.** Ventral view. **e, k, q.** Right lateral view. **f, l, r.** Left lateral view. Tentative position along the vertebral column: **a-f** = L-b, second lumbar; **g-l** = L-c, third lumbar; **m-r** = L-d, fourth lumbar. All images were generated from three-dimensional surface models. Scale bar = 50 cm.

Extended Data Fig. 4 | Three incomplete vertebrae of *Perucetus colossus* (MUSM 3248, holotype). a, g, m. Anterior view. **b, h, n.** Posterior view. **c, i, o.** Dorsal view. **d, j, p.** Ventral view. **e, k, q.** Right lateral view. **f, l, r.** Left lateral view. Tentative position along the vertebral column: **a-f** = L-e, fifth lumbar; **g-l** = L-f, sixth lumbar; **m-r** = L-g, seventh lumbar. All images were generated from three-dimensional surface models. Scale bar = 50 cm.

Extended Data Fig. 5 | Two vertebrae (a-l) and three posterior ribs (m; R-b,c,d) of *Perucetus colossus* (MUSM 3248, holotype). a, g. Anterior view. **b, h.** Posterior view. **c, i.** Dorsal view. **d, j.** Ventral view. **e, k.** Right lateral view. **f, l** Left lateral view**.** Tentative position along the vertebral column: **a-f** = L-j, eleventh lumbar; **g-l** =L-k, twelfth lumbar. **a-l**. Images generated from three-dimensional surface models. **m.** Photograph taken in the field. Scale bars = 50 cm.

Extended Data Fig. 6 | Vertebral and costal morphology of *Perucetus colossus* (MUSM 3248, holotype) compared to that of other cetaceans. a, mean and maximum ratio of vertebral centrum anteroposterior length (CL) to mediolateral width (CW), computed with the thoracic and lumbar vertebrae of other cetaceans (Ba = Basilosaurinae; Dor = Dorudontinae; FM = fossil Mysticeti; FO = fossil Odontoceti; P = Pakicetidae+Ambulocetidae; Pa = Pachycetinae; Pr = Protocetidae; R = Remingtonocetidae). **b,** profile of vertebral centrum length in *P. colossus* (Gt) compared with the profiles of other basilosaurids (Aa = *Antaecetus aithai*; Bc = *Basilosaurus cetoides*; Bc = *Basilosaurus isis*; Cf = *Chrysocetus fouadassii* Cp = *Cynthiacetus peruvianus*; Da = *Dorudon atrox*; data of *A. aithai* and *B. isis* from Gingerich et al.[15], fig. 11). **c,** curvature (length/chord) of the best preserved rib (red horizontal line) compared to those of *Cynthiacetus peruvianus* (MNHN.F.PRU10).

Extended Data Fig. 7 | Vertebral microanatomy illustrated with binarized sections (black = bone) obtained with physical core drills (a) or µCT data (b-f). a, *Perucetus colossus* (MUSM 3248, holotype, vertebra L-e for the centrum and transverse process and L-c for the neural spine). The global compactness (Cg) was measured in ten areas (orange outlines) to assess overall centrum compactness (see Supplementary Methods). **b**, common minke whale (*Balaenoptera acutorostrata*, LR M 523). **c**, Amazon river dolphin (*Inia geoffrensis*, ZMB_Mam_41500). **d**, common dolphin (*Delphinus* sp. ZMB_Mam_697.59). **e**, dugong (*Dugong dugon,* ZMB_Mam_69340). **f**, manatee (*Trichechus manatus*, ZMB_Mam_17377). **(1)** Centrum (anteroposterior mid-length, from its dorsal edge to its centre), external towards top; **(2)** Neural spine (dorsoventral mid-height), external towards right); **(3)** Transverse process (mediolateral mid-width), external towards top. Width of the virtual cross-sections were defined as representing 7.2% of the centrum dorsoventral height; this is the mean ratio between the centrum height of *P. colossus* and the width of the physical core drills. The core drills of the neural spine and transverse process do not reach the middle of the corresponding vertebral parts (but break surfaces indicate uniform structure throughout). See core drills' location in Fig. S6b,c. Scale bars: a = 13.9 mm, b = 23.6 mm, c = 2.2 mm, d = 2.7 mm, e = 3.2 mm, f = 3.0 mm.

Extended Data Fig. 8 Estimates of the osteological range of motion. Extension and flexion of the preserved portion of vertebral column of *Perucetus colossus* holotype (MUSM 3248) is compared with an equivalent vertebral column portion of Cy*nthiacetus peruvianus* holotype (MNHN.F.PRU10) using the respective 3D models. Intervertebral spaces were reconstructed based on the common dolphin (*Delphinus delphis*)[78] (see Methods). Scale bar = 50 cm.

Extended Data Fig. 9 | Estimating the whole skeletal volume of *Perucetus colossus* based on Cy*nthiacetus peruvianus*' holotype (MNHN.F.PRU10). **a.** Unmodified 3D model of Cy*nthiacetus peruvianus*' holotype. **b, c.** vertebral column scaled-up (top) and dilated (bottom). **c, d.** Rib cage scaled-up (top) and dilated (bottom) identifying the scanned rib of *P. colossus* as R17 (**c**) or R20 (**d**). Scale bars = 2 m.

Extended Data Fig. 10 | Reconstruction of *Perucetus colossus* in its coastal habitat. Because portions of the skeleton are unknown, several aspects of the reconstruction are tentative: the overall proportions of the axial postcranium are based on a close relative *Cynthiacetus peruvianus*, which was scaled-up and dilated according to the elements recovered for *P. colossus* (see Extended Data Fig. 9); the skull and limbs were only scaled-up; the tail fluke and forelimb use (bottom-walking) are based on the manatee (*Trichechus*), the extant marine mammal with the closest degree of pachyosteosclerosis in the postcranial skeleton; the hind limb of *P. colossus* was not recovered, but the anatomy of its innominate indicates the presence of a reduced, articulated leg. The associated sawfish (*Pristis*) was recovered from the same unit in the East Pisco Basin, the Yumaque Member of the Paracas Formation[84]. Reconstruction by A. Gennari.

Methods

Geological age of *Perucetus colossus*

A stratigraphic section was measured at the type locality, starting from the base of the outcrop, which is locally marked by two dolomite layers within the Yumaque member of the Paracas Formation. The lower 18.5 m of the section are made of silt that transition upward to fine silt-clay. The base of the Otuma Formation occurs at 34.5 m; it is followed by two ash layers interbedded with fine silt-clay (Extended Data Fig. 1). The holotype of *P. colossus* occurs some metres below the basal Otuma strata, ca. 30 m above the base of the section.

Samples for biostratigraphic analyses were prepared as standard smear-slides and analysed with an Olympus BX50 polarised light microscope at 1000× with immersion oil. The identification of calcareous nannofossils followed the taxonomy of Perch-Nielsen[49] and Young et al.[50]. Zonal schemes are based on Martini[51], with zonal codes NP, and Agnini et al.[52], with zonal codes CNE.

For the ^{39}Ar–^{40}Ar dating analyses, a 10-cm-thick volcanic ash layer was sampled ca. 5 m above the level of the fossil specimen (Extended Data Fig. 1), avoiding weathered and extraneous particles. The collected tephra was petrographically analysed under a stereomicroscope and a Leica optical microscope after preparing smear slides. Grain-size analyses were performed with a Malvern Mastersizer 2000E™Laser Granulometer and data were processed with the grain-size analysis program GRADISTAT 4.0[53] at the Università degli Studi di Milano-Bicocca. The ash sample was wet-sieved through meshes of 500, 250, 125, and 63 µm, and the 250–500 µm fraction was mounted in resin and polished for compositional analyses through a JEOL 8200 Superprobe™ at the Università degli Studi di Milano Statale, with 15 kV accelerating voltage and 5 nA beam current. The beam diameter was 3 µm for biotite phenocrysts and 10 µm for glass shards. Finally, biotite phenocrysts were collected by handpicking and irradiated in the McMaster University nuclear reactor. They were analysed through the NuInstruments™ Noblesse® noble gas mass spectrometer at the Università degli Studi di Milano-Bicocca by stepwise heating, following Bosio et al.[54]. See Supplementary Methods for details on the lithostratigraphy, biostratigraphy, palaeoenvironmental setting and ^{39}Ar–^{40}Ar dating analyses.

Vertebral proportions in Cetacea

Centrum length and width of the thoracic and lumbar vertebrae were compiled for extant[55] and extinct cetaceans (Supplementary Data 3). The mean and maximum values of the length/width ratio (CL/CW) were then compared to those of *P. colossus* (Extended Data Figure 6; R[56] package ggplot2[57]).

Bone microanatomy and histology

One of the recovered ribs and several vertebrae were sampled to produce palaeohistological thin-sections, following standard procedures[58,59]. A half cross-section was made around the rib's mid-length. For the vertebrae, we used core drillings to sample the centrum (in both the anteroposterior and dorsoventral directions), neural spine, and transverse processes (see also Supplementary Methods). Break surfaces were opportunistically observed for all recovered elements.

The obtained thin-sections were observed and photographed with a petrographic microscope (Leica DM750P) equipped with a camera (Leica ICC50 W) under natural and cross-polarized light for detailed views. A Keyence system (VH-Z20R objective) was used to capture general views of the sections. To measure the global compactness of each section, images were thresholded manually (so that bone tissue represents the foreground, and the rest the background). Compactness was then measured as the ratio between the foreground and background areas within a selection corresponding to the whole cross-sectional area ('Measure' routine of Fiji/ImageJ[60,61]; Supplementary Table 2).

Extensive comparative material for rib cross-sections has already been published[5,13,14,62,63]. For the microanatomy of the vertebra, the regions sampled in the new specimen were examined in extant cetaceans and sirenians through virtual thin-sections (Extended Data Fig. 7; Supplementary Table 2) using high resolutions CT-scans from existing datasets[64,65]. These sections were produced using a rectangular region of interest (ROI) corresponding to the regions sampled on the fossils; these ROIs were extracted, thresholded, and their bone compactness was measured with Fiji/ImageJ[60,61] [‘Rotate’, ‘Orthogonal views, ‘Threshold’ (with stack histogram option), ‘Measure’, routines]. The longer side of the VOI was defined from the periosteal surface to the middle of the region (e.g., mid-length of the centrum); its shorter side was set proportionally to the diameter of core drilled in the fossil, i.e., ca. 7.2% of the centrum’s height.

Skeleton and whole body mass estimations

Dry skeletal mass (SM) is here understood as the bone tissue, excluding the free water it can contain (but including more tightly bound water[66]) as well as the adipose tissues. Skeletal fraction (SF) is defined as the ratio between SM and total body mass (BM). Several methods of SM estimations used herein will rely on compact bone density, which can vary from one species/location to another. Here we used existing data for a terrestrial mammal (*Panthera leo*), a cetacean (*Delphinus delphis*), and a sirenian (*Dugong dugon*)[67,68]. Regressing global compactness against bone density, one can estimate (lm and predict functions, base of R) the mean dry bone tissue densities (for bones of the whole skeleton) of these three animals (1.89 $g.cm^{-3}$, 2.07 $g.cm^{-3}$, and 2.12 $g.cm^{-3}$, respectively).

We used different methods to assess skeletal mass across a dataset that includes both extant and extinct amniotes. These methods include direct weighting of the skeletons (extant terrestrial mammals and some marine mammals), extrapolations based on SF for large cetaceans, based on whole skeleton volume for sauropods, extremely small amniotes, extinct sirenians, and large, extinct mammals. See Supplementary Methods and Supplementary Tables 6-16 for details.

In addition to direct body mass measurements, body masses were estimated using body measurement regressions (large cetaceans, small amniotes, sirenians), published estimations (sauropods, extinct terrestrial mammals), or taken from AnAge (for the Etruscan shrew and for the mean values of large cetaceans). See Supplementary Methods and Supplementary Tables 6, 9, and 12 for details.

Skeletal mass ~ body mass scaling

Two distinct scaling relationships were assessed, one for extant, terrestrial mammals, and one for extant cetaceans (Supplementary Tables 2, 3). Skeleton data of Prange et al[69], completed for species of BM ranging from 62 to 290 kg with newly acquired measurements. These new data are derived from wild-caught museum specimens for which body mass is known, and for which the dry skeletons were weighted with a digital scale (Supplementary Data 2). The extant cetacean data were taken from Buffrénil et al.[70], Buffrénil[71], and Robineau and Buffrénil[72] (for the *Delphinus delphis* sample only mature specimens were taken, i.e., with at least ten growth marks; see [70]).

We examined the scaling of dry skeletal mass against whole body mass through phylogenetically informed linear regressions. These regressions account for the phylogenetic relatedness of observations through the determination of the optimised Pagel's lambda value (bounded to [0;1]) of the regression (*gls* function, nlme package[73], *corPagel* function, ape package[74]. As timetree, we used the node-dated, maximum clade credibility tree from Upham et al.[75]. Sampled species were swapped with closest relatives when not already present in the tree. Pseudo-R^2 values were computed with the *rsquared* function (piecewiseSEM package[76]).

***Perucetus colossus* skeletal and body mass estimations**

The skeleton volume of *P. colossus* was estimated based on surface scans of the holotype and more complete basilosaurid skeletons. The 3D surface textured models of the holotype were created using a SHINING EinScan Pro HD handheld scanner for the vertebrae and an Artec Eva scanner for the rib and innominate (both at the highest resolution: 0.25 mm and 0.5 mm, respectively). The volume of each model was measured (Blender 3.0.1[77]), substracting that of the sediment still filling the neural canal of some vertebrae. In addition to being used in the following steps, the vertebrae' volume was compared to those of the Wexford blue whale (NHMUK-ZD.1892.3.1.1) and to a cast of a posterior thoracic/lumbar vertebra of *Basilosaurus cetoides* (Liège University, made with an Artec Spider surface scanner).

To estimate the volume of the unpreserved skeletal elements, we used as a base the most complete and best preserved skeleton of basilosaurid, that of *Cynthiacetus peruvianus*' holotype (MNHN.F.PRU10; surface scanned with an Artec Eva scanner). We made several estimations based on this skeleton: 1. Scaling up and dilating *C. peruvianus*' skeleton for the corresponding bone to reach the volume of those of *P. colossus'* holotype (Extended Data Fig. 10). Because the precise position of the recovered skeletal elements is unknown, 10,000 random draws were made to select corresponding vertebrae in the posterior thoracic and lumbar regions (see R code in Supplementary Dataset). For the rib cage, two alternatives were assessed, considering the digitised rib of *P. colossus* to correspond to the anterior-most rib with simple proximal end morphology (R17) or last rib (R20). 2. Adapting the scaled-up, dilated models based on *C. peruvianus* to fit the skeleton composition of two other well-known basilosaurids, *Basilosaurus isis*[35] and *Dorudon atrox*[17]; a conservative skeleton composition was also used, assuming minimum counts of 12 thoracic and 15 lumbar vertebrae. See Supplementary Methods and Supplementary Tables 17 and 18 for details. Skeletal length was taken from the scaled-up models (the pachyostosis does not affect the vertebral centra anteroposteriorly).

The skeletal mass was assessed using the minimum and maximum obtained volumes and the skeletal elements' density, which derived from the histological samples made on *P. colossus'* holotype (vertebrae and ribs, which represent over 97% of the skeleton's volume) or an extant cetacean, *Delphinus delphis* (rest of the skeleton; Supplementary Methods and Supplementary Tables 19 and 20).

Finally, the body mass of *P. colossus* was estimated based on the skeletal fractions (SF; skeletal mass to whole body mass ratio) of extant species. These skeletal fractions inform on the viable proportion of tissues in these animals, and overall body density is particularly critical for aquatic vertebrates, especially amniotes who regularly have to surface to breathe. We have hence used the two extreme values measured in extant, fully aquatic mammals: 2.24% *Mesoplodon europaeus*[72] and 6.25 % for *Trichechus manatus* (mean of adults from Domning & Buffrénil[26]; Supplementary Table 22), as well as the mean value for cetaceans, whose SF scaling differs from that of other mammals.

Estimating range of motion of the vertebral column

Using a methodological approach similar to that applied to crocodylomorphs by Molnar et al.[39], we estimated the osteological range of motion in ventral flexion, dorsal extension and lateral flexion of the preserved portion of vertebral column of *P. colossus* and of an equivalent vertebral portion of column of *C. peruvianus*. To take into account also the effect on flexibility of the length of the vertebral centra, we selected a portion of the vertebral column of *C. peruvianus* having the centrum of the middle vertebra with the same width as that of the *P. colossus*. Thus, due to the shorter centra, the number of vertebrae selected for *C. peruvianus* was greater (18) than those of *P. colossus* (13). The osteological range of motion was estimated by manipulating the virtual 3D models of *P. colossus* and C. *peruvianus* holotypes in Blender 3.0.1[77]. The missing parts of the 13 vertebrae of *P. colossus* were virtually reconstructed by copying and adapting the respective preserved parts of the adjacent vertebrae. Intervertebral spacing was estimated for both species using the intervertebral discs' proportions of *Delphinus delphis*[78].

Data availability

All data and code generated or analysed during this study are included in this published article (and its supplementary information files). Three-dimensional surface models of the holotype of *P. colossus* as well as *Cynthiacetus peruvianus* MNHN.F.PRU10 are available on MorphMuseum [temporary links: http://morphomuseum.com/Specimenfiles/sendFile/1131/d7a008; http://morphomuseum.com/Specimenfiles/sendFile/1130/154c7f]. Newly acquired CT data are available on Morphosource [temporary link: http://n2t.net/ark:/87602/m4/510260].

References

49. Perch-Nielsen. Cenozoic Calcareous Nannofossils. in *In Plankton Stratigraphy* (eds. Bolli, H. M., Saunders, J. . & Perch-Nielsen, K.) 427–554 (1985).

50. Young, J. R., Bown, P. R. & Lees, J. A. Nannotax3 website. *International Nannoplankton Association. http://www.mikrotax.org/Nannotax3* (2022).

51. Martini, E. Standard Tertiary and Quaternary calcareous nannoplankton zonation. in *Proceedings 2nd International Conference Planktonic Microfossils* (ed. Farinacci, A.) vol. 2 739–785 (1971).

52. Agnini, C. *et al.* Biozonation and biochronology of Paleogene calcareous nannofossils from low and middle latitudes. *Newsletters Stratigr.* **47**, 131–181 (2014).

53. Blott, S. J. & Pye, K. GRADISTAT: a grain size distribution and statistics package for the analysis of unconsolidated sediments. *Earth Surf. Process. Landforms* **26**, 1237–1248 (2001).

54. Bosio, G. *et al.* Tephrochronology and chronostratigraphy of the Miocene Chilcatay and Pisco formations (East Pisco Basin, Peru). *Newsletters Stratigr.* **53**, 213–247 (2020).

55. Gillet, A., Frédérich, B. & Parmentier, E. Divergent evolutionary morphology of the axial skeleton as a potential key innovation in modern cetaceans. *Proc. R. Soc. B Biol. Sci.* **286**, 20191771 (2019).

56. R Core Team. R: A language and environment for statistical computing. at https://www.r-project.org/ (2021).

57. Wickham, H. ggplot2: Elegant graphics for data analysis. at https://ggplot2.tidyverse.org (2016).

58. Padian, K. & Lamm, E.-T. Bone histology of fossil tetrapods : advancing methods, analysis, and interpretation. in 285 (University of California Press, 2013).

59. Stein, K. & Sander, P. M. Histological Core Drilling: a Less Destructive Method for Studying Bone Histology. *Methods Foss. Prep. Proc. First Annu. Foss. Prep. Collect. Symp.* 69–80 (2009).

60. Schneider, C. A., Rasband, W. S. & Eliceiri, K. W. NIH Image to ImageJ: 25 years of image analysis. *Nat. Methods* **9**, 671–675 (2012).

61. Schindelin, J. *et al.* Fiji: an open-source platform for biological-image analysis. *Nat. Methods* **9**, 676–682 (2012).

62. Canoville, A., Buffrénil, V. de & Laurin, M. Microanatomical diversity of amniote ribs: an exploratory quantitative study. *Biol. J. Linn. Soc.* **118**, 706–733 (2016).

63. Hayashi, S. *et al.* Bone inner structure suggests increasing aquatic adaptations in Desmostylia (Mammalia, Afrotheria). *PLoS One* **8**, e59146 (2013).

64. Amson, E. & Bibi, F. Differing effects of size and lifestyle on bone structure in mammals. *BMC Biol.* **19**, 87 (2021).

65. Dumont, M. *et al.* Inner architecture of vertebral centra in terrestrial and aquatic mammals: A two-dimensional comparative study. *J. Morphol.* **274**, 570–584 (2013).

66. Surowiec, R. K., Allen, M. R. & Wallace, J. M. Bone hydration: How we can evaluate it, what can it tell us, and is it an effective therapeutic target? *Bone Reports* **16**, 101161 (2022).

67. Buffrénil, V. de, Sire, J.-Y. & Schoevaert, D. Comparaison de la structure et du volume squelettiques entre un delphinidé (*Delphinus delphis* L.) et un mammifère terrestre (*Panthera leo* L.). *Can. J. Zool.* **64**, 1750–1756 (1986).

68. Buffrénil, V. de & Schoevaert, D. Données quantitatives et observations histologiques sur la pachyostose du squelette du dugong, *Dugong dugon* (Müller) (Sirenia, Dugongidae). *Can. J. Zool.* **67**, 2107–2119 (1989).

69. Prange, H. D., Anderson, J. F. & Rahn, H. Scaling of skeletal mass to body mass in birds and mammals. *Am. Nat.* **113**, 103–122 (1979).

70. Buffrénil, V. de, Collet, A. & Pascal, M. Ontogenetic development of skeletal weight in a small delphinid, *Delphinus delphis* (Cetacea, Odontoceti). *Zoomorphology* **105**, 336–344 (1985).

71. Buffrénil, V. de. Contribution à l'étude des spécialisations de la structure osseuse des mammifères marins. (Thèse de doctorat ès sciences, Université Paris VII , Paris, 1990).

72. Robineau, D. & Buffrénil, V. de. Nouvelles données sur la masse du squelette chez les grands cétacés (Mammalia, Cetacea). *Can. J. Zool.* **71**, 828–834 (1993).

73. Pinheiro, J., Bates, D., DebRoy, S., Sarkar, D. & R Core Team, . nlme: Linear and nonlinear mixed effects models. R package. at (2016).

74. Paradis, E., Claude, J. & Strimmer, K. APE: Analyses of phylogenetics and evolution in R language. *Bioinformatics* **20**, 289–290 (2004).

75. Upham, N. S., Esselstyn, J. A. & Jetz, W. Inferring the mammal tree: Species-level sets of phylogenies for questions in ecology, evolution, and conservation. *PLOS Biol.* **17**, e3000494 (2019).

76. Lefcheck, J. S. piecewiseSEM: Piecewise structural equation modelling in R for ecology, evolution, and systematics. *Methods Ecol. Evol.* **7**, 573–579 (2016).

77. Blender Online Community. Blender - a 3D modelling and rendering package. at http://www.blender.org (2018).

78. Long, J. H., Pabst, D. A., Shepherd, W. R. & McLellan, W. A. Locomotor design of dolphin vertebral columns: Bending mechanics and morphology of *Delphinus delphis*. *J. Exp. Biol.* **200**, 65–81 (1997).

79. Travis, R. B., Gonzales, G. & Pardo, A. Hydrocarbon potential of coastal basins of Peru. in *Circum-pacific energy and mineral resources* (eds. Halbouty, M., Mahe, J. & Lian, H. M.) 331–338 (1976).

80. Thornburg, T. & Kulm, L. D. Sedimentary basins of the Peru continental margin: Structure, stratigraphy, and Cenozoic tectonics from 6°S to 16°S latitude. *Mem. Geol. Soc. Am.* **154**, 393–422 (1981).

81. Malinverno, E. *et al.* (Bio)stratigraphic overview and paleoclimatic-paleoceanographic implications of the middle-upper Eocene deposits from the Ica River Valley (East Pisco Basin, Peru). *Palaeogeogr. Palaeoclimatol. Palaeoecol.* **578**, 110567 (2021).

82. Bianucci, G. & Collareta, A. An overview of the fossil record of cetaceans from the East Pisco Basin (Peru). *Boll. della Soc. Paleontol. Ital.* **61**, 19–60 (2022).

83. Bosio, G. *et al.* Ultrastructure, composition, and 87Sr/86Sr dating of shark teeth from lower Miocene sediments of southwestern Peru. *J. South Am. Earth Sci.* **118**, 103909 (2022).

84. Collareta, A. *et al.* A rhinopristiform sawfish (genus *Pristis*) from the middle Eocene (Lutetian)

of southern Peru and its regional implications. *Carnets de géologie* **20**, 91–105 (2020).

Acknowledgements

We warmly thank A. Ball, L. Cornish, and R. Sabin for access to the Wexford blue whale model and related data, A. Martinez Luna for his help with the core drilling, A. Risplendente for EPMA analysis on biotite, A. Gioncada for tephra analyses, A. Larramendi for his advice with body density analyses, C. Wimmer-Pfeil and S. Morel for preparing the thin-sections, D. Hagmann and J. Schaeffer, G. Billet, F. Zachos, and U. Göhlich for their help with surface models, E. Steurbaut for preliminary biostratigraphic investigation, F. Goussard for capturing the surface model of *C. peruvianus*' holotype, G. Bagnoli, C. Chacaltana, T.J. DeVries, K. Gariboldi, W. Landini, G. Molli, and G.i Sarti for fruitful discussions about the geology and palaeontology of the East Pisco Basin, G. Carnevale for fossil fish identifications, N. Fusi for grain-size analysis, Q. Martinez for discussions and help with CT data acquisition, V. Barberini for the assistance in ^{39}Ar-^{40}Ar dating, V. Fischer for the surface model of a vertebra of *Basilosaurus cetoides*, V. de Buffrénil and D. Germain for sharing CT data, W. Aguirre Diaz for the fossil preparation, and A. Altamirano, A. Martinez Luna, E. Diaz Ramoz, J. Chauca-Luyo, M. Laime Molina, G. Olmedo, M. Burga, N. Ramirez, Piero Giuffra, R. Varas-Malca, W. Aguirre Diaz, for field fossil collection and laboratory assistance, and two anonymous reviewers for their help improving the manuscript. The stay of R.B. at the MUSM has been funded by a Stan Wood Award from the Palaeontological Association. Grants from the University of Pisa (PRA_2017_0032 to G. Bi.) and the University of Camerino (FAR 2019, STI000102 to C.DiC.) supported this work.

Authors contribution

M.U. discovered and collected the fossil. E.A., G.Bi., and O.L. conceived and designed the project. G.Bo., A.C., C.Di C., E.M., I.M.V., and P.P.P. collected and analysed the stratigraphical data and wrote the corresponding methods sections. A.B., A.C., E.A., G.Bi., M.M., O.L., R.B., and R.S.-G., collected phenotypic data (including CT and/or surface scans and/or palaeohistological samples). E.A., G.Bi., and O.L. analysed the phenotypic data. E.A., G.Bi., and O.L. wrote the first draft of the manuscript. All authors discussed the analyses and reviewed the manuscript.

Competing interests

The authors declare no competing interests.

Material and correspondence

E.A.

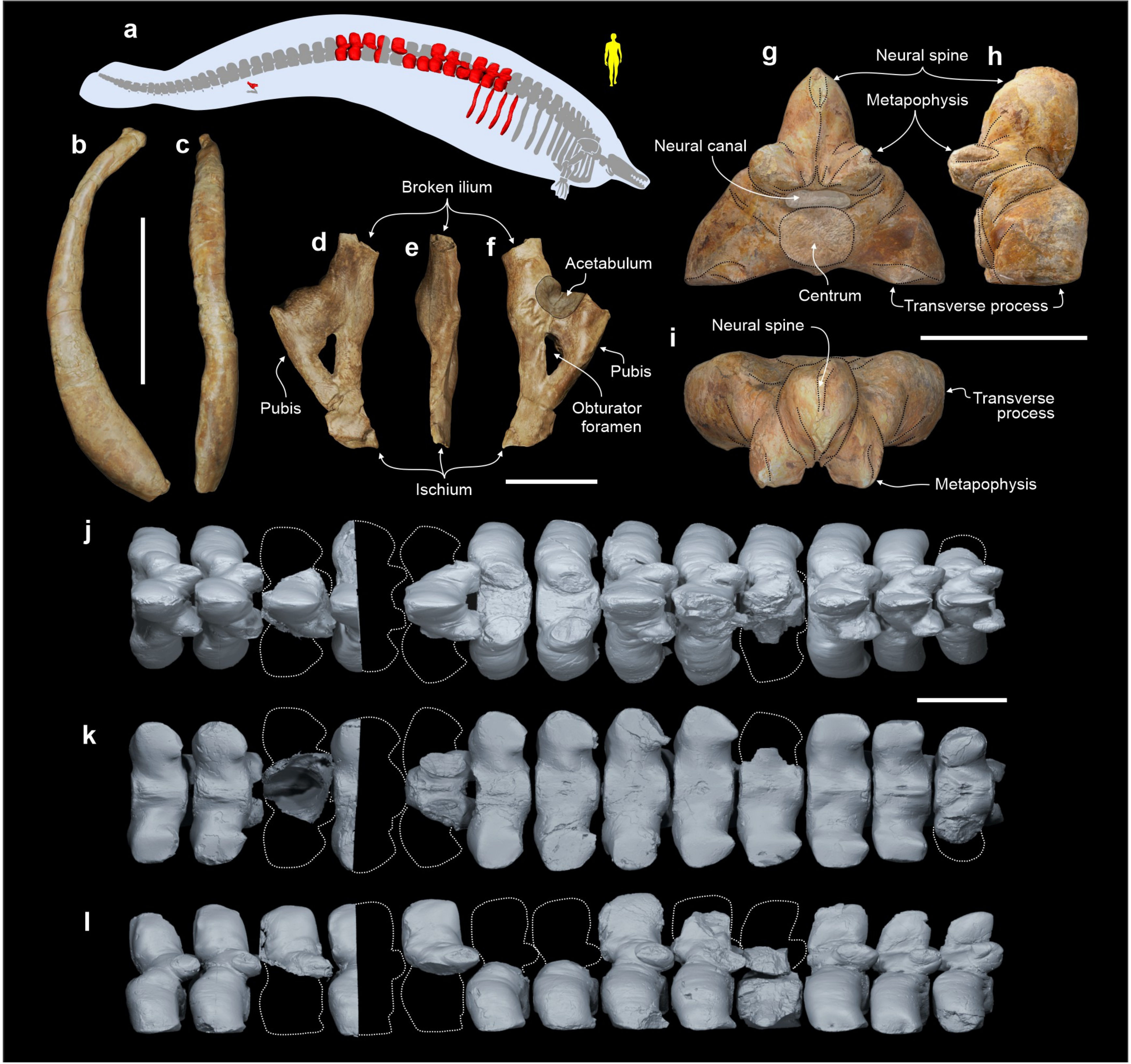
a
b
c
Broken ilium
d
e
f
Acetabulum
Pubis
Pubis
Obturator foramen
Ischium
g
Neural spine
h
Metaphysis
Neural canal
Centrum
Transverse process
i
Neural spine
Transverse process
Metapophysis
j
k
l

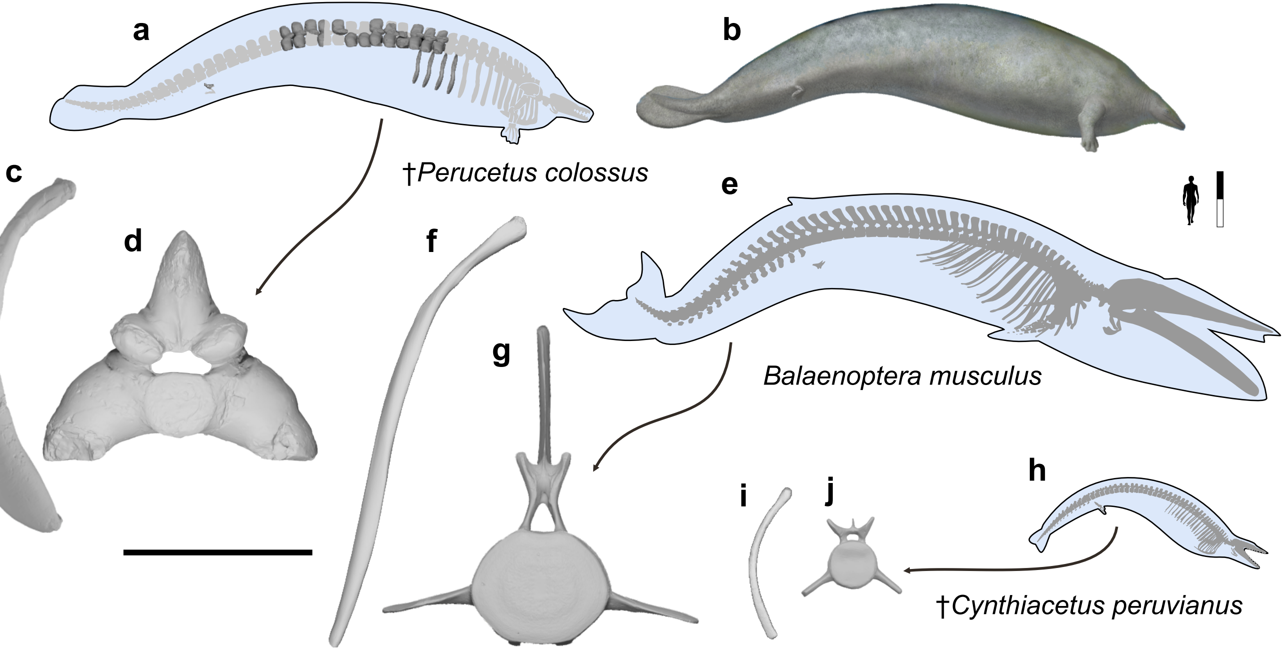
a
b
†Perucetus colossus
c
d
e
f
g
Balaenoptera musculus
h
i
j
†Cynthiacetus peruvianus

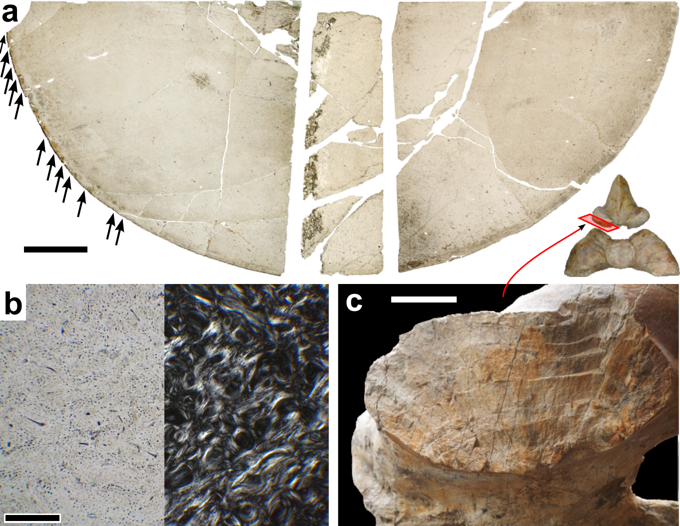
a
b
c

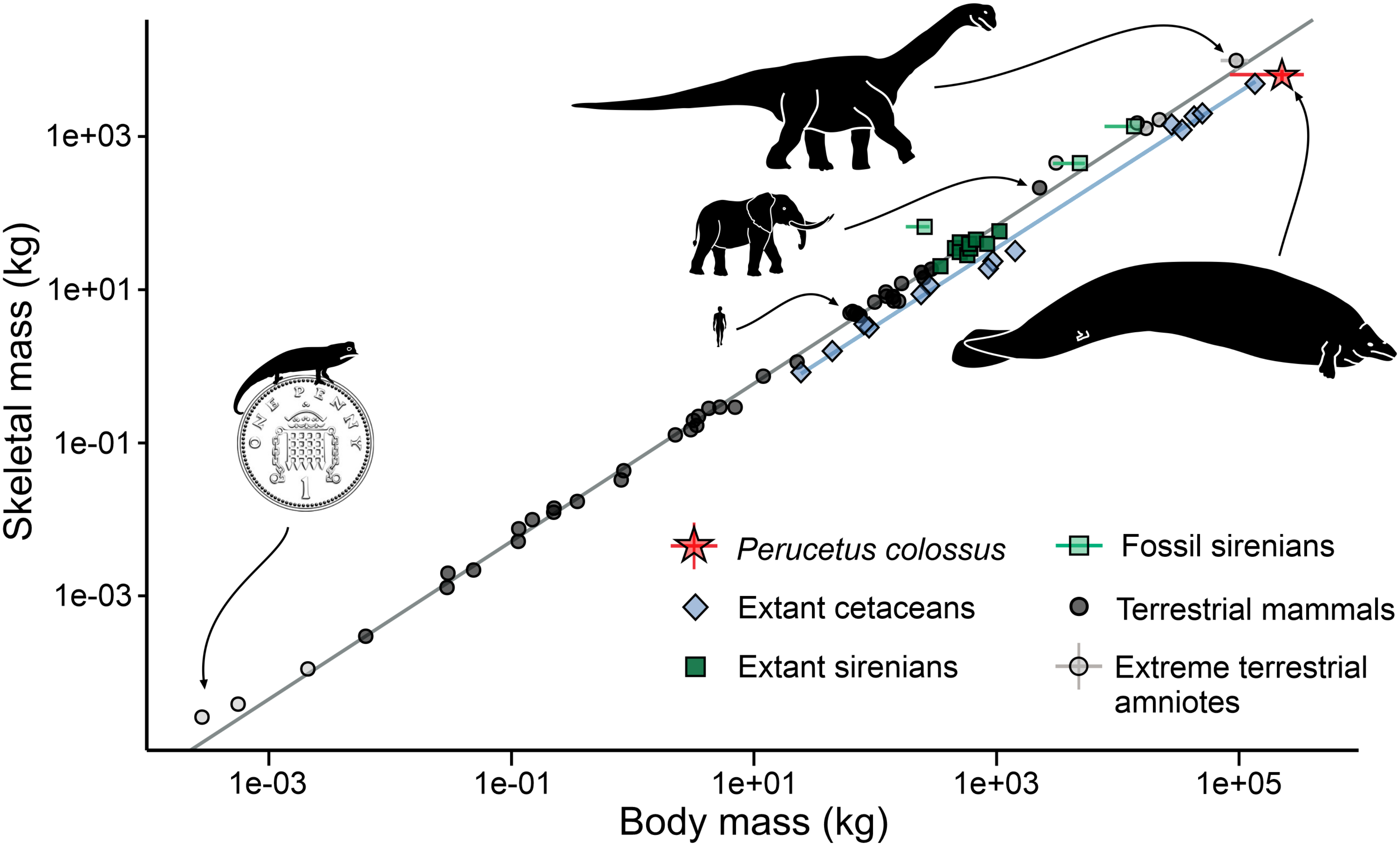
Skeletal mass (kg)
1e+03
1e+01
1e-01
1e-03
Body mass (kg)
1e-03
1e-01
1e+01
1e+03
1e+05
ONE PENNY
1
Perucetus colossus
Extant cetaceans
Extant sirenians
Fossil sirenians
Terrestrial mammals
Extreme terrestrial amniotes